Int. J. Electrochem. Sci., 14 **(2019)** 7332 – 7347, doi: 10.20964/2019.08.87

International Journal of
ELECTROCHEMICAL
SCIENCE
www.electrochemsci.org

Corrosion Behavior of P110 Steel in Simulated Oilfield Produced Water

Xuchao Chen[1], *Zichao Guan*[1], *Min Du*[1,*], *Cunguo Lin*[2,*]

[1] The Key Laboratory of Marine Chemistry Theory and Technology, Ministry of Education, College of Chemistry and Chemical Engineering, Ocean University of China, Qingdao 266100, People's Republic of China
[2] State Key Laboratory for Marine Corrosion and Protection, Luoyang Ship Material Research Institute (LSMRI), Qingdao 266237, People's Republic of China
[*]E-mail: sdm06@126.com; lincg@sunrui.net

Received: 10 April 2019 / *Accepted:* 21 May 2019 / *Published:* 30 June 2019

Corrosion behavior of P110 steel in simulated oilfield produced water was researched by weight loss, electrochemical methods and surface analysis methods. Effects of temperature and CO_2 partial pressure were discussed. Weight loss experiment results showed that the corrosion rates increased firstly and then decreased gradually with temperature, and reached maximum at 60℃. The effect of CO_2 was more obvious at low temperature, and the effect weakened with the increasing of temperature. General corrosion took advantage at low temperature. But local corrosion appeared at temperatures higher than 90℃. According to the electrochemical analysis, the corrosion rates increased with immersing time at 60℃. However, the corrosion rates decreased with the corrosion proceeding at 90℃. Surface analysis shows the incomplete $FeCO_3$ film enhanced the general corrosion at 60℃. When the temperature raised to 90℃, the corrosion products were Fe_2O_3 and $Mg_3Ca(CO_3)_4$. Although the compact Fe_2O_3 film restrained the general corrosion, the existence of $Mg_3Ca(CO_3)_4$ induced the pitting corrosion.

Keywords: CO_2 Corrosion, P110 Steel, Simulated Oilfield Produced Water

1. INTRODUCTION

In recent years, more and more oilfield produced water was produced which has much salinity, higher temperature and CO_2 concentration, so the corrosion rates of metals were enhanced commonly [1-3]. P110 steel is extensively used in the oil industry as oil casing. The corrosion of P110 steel is extremely serious because of the harsh environment of oil casing. Therefore, it is important to study the corrosion of P110 steel in oilfield produced water.

A great many researchers [4-7] have proposed that increasing temperature could build up the occurrence of corrosion by accelerating chemical reactions, electrochemical reactions, and mass transfer process. Zhu [8] believed that temperature can influence the corrosion rate of steel matrix and the precipitation of $FeCO_3$. Honarvar [9] claimed that the threshold temperature of forming $FeCO_3$ layer was 65℃. The apparent density and thickness of $FeCO_3$ scale were advanced by increasing temperature. Mendili [10] and Li [11] confirmed a conclusion that the environmental temperature affected the steel corrosion by controlling the formation and diversification of the corrosion products film.

The CO_2 partial pressure is another key factor for CO_2 corrosion. It has been recognized that CO_2 corrosion is one of the most serious corrosion types in oil well[12]. Carbon dioxide gas hydrates in water and changes into carbonic acid, which is more harmful than hydrochloric acid at the same pH level. Many researchers [12-15] thought that CO_2 partial pressure was a critical factor for CO_2 corrosion, so it was usually used as a criterion to evaluate the corrosively. Although the change of CO_2 partial pressure does not change the corrosion mechanism, the corrosion rates of X65 pipeline steel under high CO_2 partial pressure are much higher than that at low CO_2 partial pressure [16]. Besides, the CO_2 partial pressure has the ability to change the type of corrosion. When the CO_2 partial pressure increases to 4 MPa, the corrosion type became localized corrosion[11]. Choi [17] obtained information about the CO_2 corrosion characteristics of deep water oil production tubing material with the condition of high temperature and pressure. Serious pitting corrosion was found on the specimens at about 90℃. They deemed that the primary determinant of corrosion style was temperature, and the CO_2 partial pressure had the power to accelerate the pitting corrosion.

With the exploration of oil wells going deeper, the carbon steels are exposed to higher pressure, higher temperature, and a more corrosive environment with the partial pressure of acidic gas CO_2 increasing exponentially with depth. However, to date, the work on the corrosion of P110 steel which always used to be oil casing in oilfield with high CO_2 partial pressure under high temperature and pressure is insufficient. In this work, the corrosion behavior of P110 steel in oilfield produced water was investigated, and the corrosion mechanism was also explored.

2. EXPERIMENTAL MATERIALS AND METHODS

The experimental material was P110 steel, which is commonly used in oilfield casing system. Its composition (wt %) is listed in Table 1.

Table 1. Chemical Composition of Tested P110 Steels (mass, %)

Material	C	Si	Mn	Cr	Mo	P	Ni	S	Fe
P110	0.25	0.20	1.40	0.15	0.01	0.01	0.012	0.003	Margin

The simulated oilfield produced water was prepared by analytical reagents and deionized water. Its chemical composition is shown in Table 2.

Table 2. Chemical Composition of Simulated Oilfield Produced Water (g/L)

Composition	Na_2CO_3	$NaHCO_3$	Na_2SO_4	$CaCl_2$	$MgCl_2$	KCl	NaCl
Content	0.0322	3.0638	1.1096	0.5053	1.6603	0.3553	16.6172

2.1 Weight loss test

Weight loss tests were conducted in a ZCF-2L autoclave made from Ti alloy to investigate corrosion rates of P110 steel. The test specimens were machined to a size of 50mm×10mm×3mm. Tests were carried out in the autoclave at total pressure of 5.0 MPa for 72 h. The detailed test conditions of weight loss tests were as follows: five temperatures of 40, 60, 80, 90, and 110°C, four CO_2 partial pressures of 0.5, 1.0, 2.5, and 4.0 MPa. Three equivalent specimens were used in each test in order to ensure the reproducibility. 1.4L simulated oilfield produced water was added in the autoclave and the total volume of autoclave was 2L. Before the tests, high purity (99.99%) nitrogen gas was immitted into the autoclave for 2h to remove dissolved oxygen from the solution. The specimens were cleaned with distilled water and ethanol, dried, and weighted using FA2004N-digit electronic balance with a precision of 0.1mg. Their dimensions were measured accurately with a vernier caliper before weight loss test.

After the test was completed, the corroded specimens were rinsed with distilled water. The corrosion products were removed with the deruster containing hexamethylenetetramine and hydrochloric acid, and then rinsed and dried again. The corrosion rate V_{corr} (mm/a) was calculated by the following formulas:

$$R_{mass} = \frac{m_0 - m_t}{S_0 t} \text{ (g/(m}^2\text{·h))} \quad (1)$$

$$V_{corr} = \frac{R_{mass}}{\rho} \times \frac{24\times365}{1000} = 8.76 \times \frac{R_{mass}}{\rho} \text{ (mm/a)} \quad (2)$$

Where m_0 and m_t are the original weight and final weight of specimens, respectively, g; S_0 is the exposed surface area of specimens, m^2; t represents the immersion time, h; and ρ is the steel density, g/cm^3.

2.2 Electrochemical measurement

Electrochemical measurements were performed with a three-electrode cell through a GAMRY (USA) electrochemical workstation. The working electrodes were cut into 10mm×10mm×3mm plates and then coated with epoxy so that only one 10mm×10mm face was exposed to the solution. A platinum plate was used as counter electrode, and the reference electrode was an $Ag/AgCl/Cl^-$ electrode, which was a specially designed solid electrode for high pressure test.

Prior to electrochemical measurements, the electrode was immersed in the test solution for a while until steady-state corrosion potential was reached. The experiments were repeated for several times to ensure the reproducibility. Electrochemical impedance spectroscopy (EIS) were measured at open circuit potential (OCP) by an applying a sinusoidal voltage signal of 5 mV in a frequency range of 100 kHz to 10 mHz. The results of EIS measurements were analyzed by Zview software with a suitable equivalent circuit model. Potentiodynamic polarization curves were measured by scanning at the potential from -200mV to +200mV vs. OCP and the sweep rate was 40mV/min.

2.3 Surface analysis

The surface morphology was characterized by a JSM-6700F scanning electron microscope (SEM) and corrosion products were analyzed by D8 ADVANCE X-ray Diffraction (XRD). The sizes of pits exiting on the specimens were measured with 3D Confocal Laser Scanning Microscope (CLSM) of LEXT OLS4000.

3. RESULTS AND DISCUSSION

3.1 Weight loss test

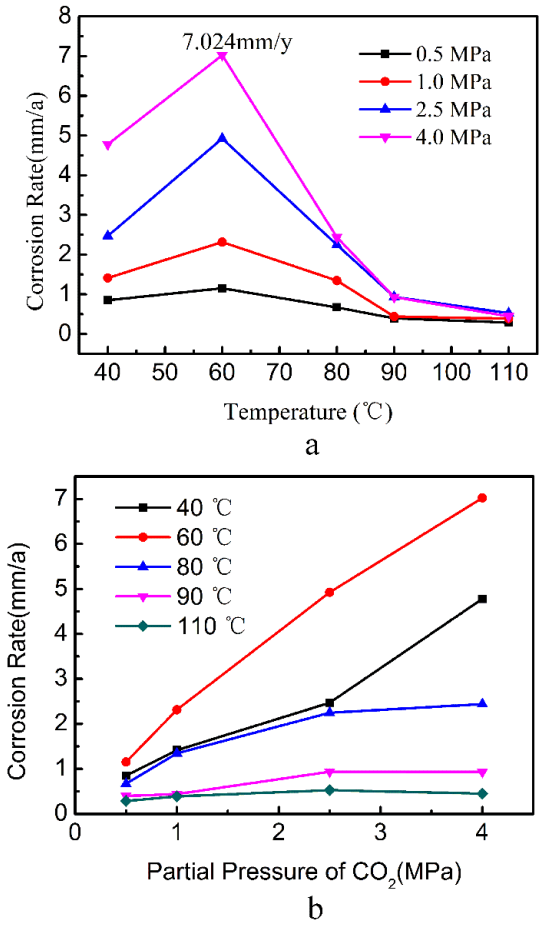

Figure 1. Corrosion rates of P110 steels in stimulate oilfield produced water at different conditions

Figure 1a shows the values of corrosion rate obtained from weight loss tests as the function of temperature in simulated oilfield produced water. The average corrosion rate was used in the paper. It shows that, in all cases of CO_2 partial pressure, the corrosion rates of P110 steel increased from 40℃ to 60℃ and the biggest appeared at 60℃. The highest corrosion rate was up to 7.024 mm/a when the CO_2 partial pressure was 4.0 MPa. Then, the corrosion rates decreased sharply from 60℃ to 90℃ and reached a relatively stable value between 90℃ and 110℃. At 110℃, the steel corrosion rates were almost equal in the four CO_2 partial pressure conditions. Some similar results were also reported by Yucheng Zhang[16], Y Xiang[18] and Choi[19].

Figure 1b shows the corrosion rates of P110 steel in simulated oilfield produced water at different CO_2 partial pressure. The result indicates that the corrosion rates increased with the increasing of CO_2 partial pressure. At a constant temperature, the CO_2 partial pressure affected corrosion process significantly by determining the type of protective scale[20]. Overall, with the change of temperature, CO_2 partial pressure affected the rates of metal corrosion in different degree. At low temperature (40℃, 60℃ and 80℃), CO_2 partial pressure had a substantial impact on the corrosion rates. The influence of CO_2 partial pressure on corrosion rates became weak when the test temperature exceeded 80℃, and it could hardly affect the corrosion rates at 110℃.

There may be two possible reasons for this result. The first is temperature. As we can know from many published literatures [21-23], conditional temperatures always try to affect steel corrosion behavior by controlling the formation and development of corrosion product film. Different corrosion products may lead to different corrosion types and affect the corrosion rates [24-28]. This reason will be discussed in detail in the following part of this paper. The second reason comes from CO_2[29]. The carbon dioxide has different solubility in simulated oilfield produced water at different temperature. As studied by Choi[19] and Deng[30], the concentrations of CO_2 and carbonic species (H_2CO_3, $HCO3^-$, and $CO3^{2-}$) decreased with temperature. At low temperature (40℃, 60℃ and 80℃), the solubility is high, and the amount of dissolved CO_2 increases with the increasing of CO_2 partial pressure, which will lead to higher corrosion rate. When the test temperature exceeded 80℃, the amount of dissolved CO_2 decreased. As a result, the corrosion rates decreased and the influence of CO_2 partial pressure moderated at the same time.

Figure 2 and Figure 3 are the surface morphology of the specimens at 80℃ and 90℃ under different CO_2 partial pressure, respectively. They are the orthograph of the specimens. As shown in Figure 2, the surfaces of specimens were quite smooth. When the temperature is less than or equal to 80 degrees, uniform corrosion occurred regardless of the pressure. Lisiane[31] found that uniform corrosion was predominant at 80℃ regardless with or without $CaCO_3$. But, in Figure 3, obvious pitting corrosion was observed on the specimens under all CO_2 partial pressure at the temperature of 90℃. With the rise of temperature, the corrosion style of P110 steel changed from general corrosion to local corrosion.

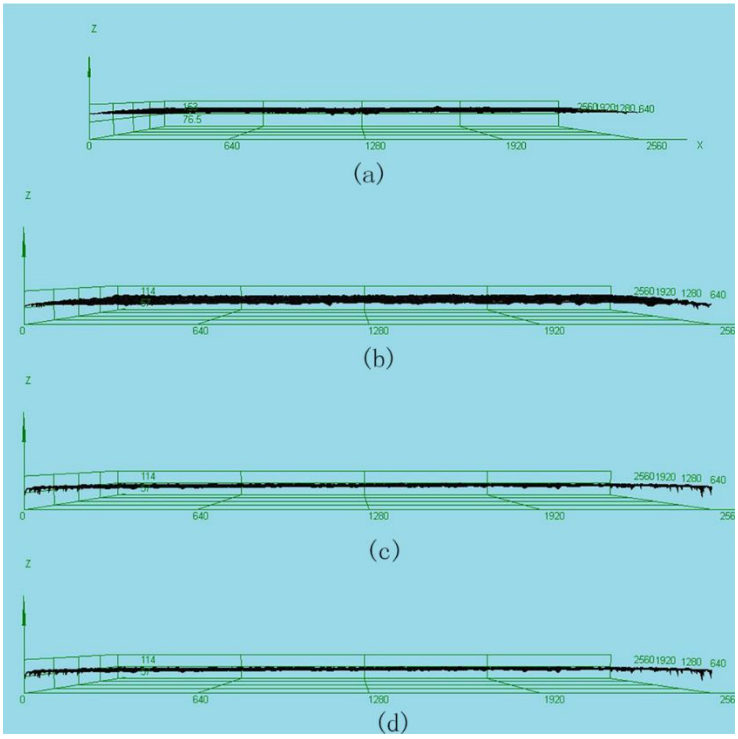

Figure 2. The morphology of the specimens at 80℃ under different CO_2 partial pressure a) 0.5MPa b) 1.0MPa c) 2.5MPa d) 4.0MPa

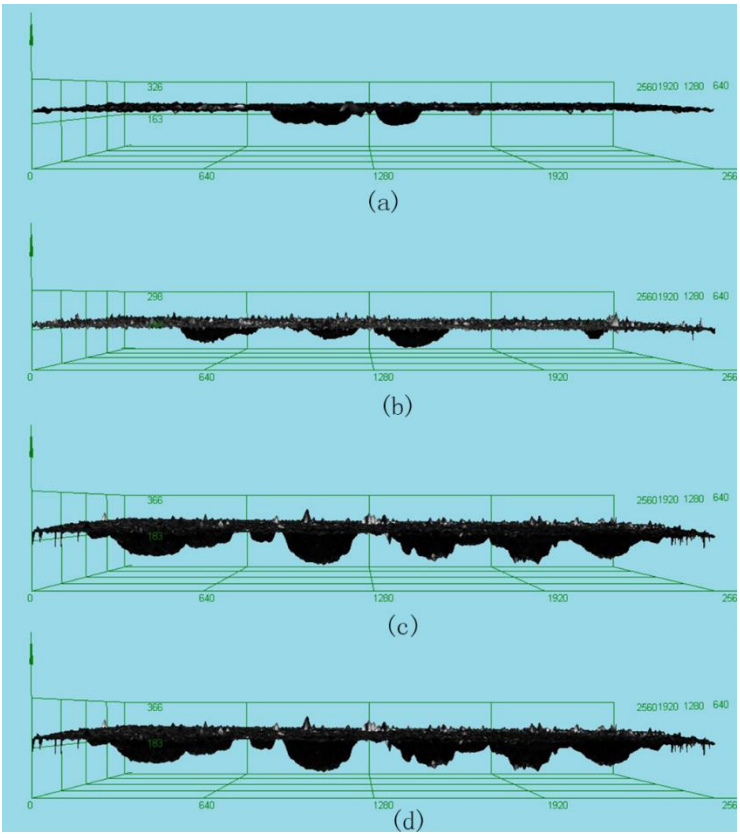

Figure 3. The morphology of the specimens at 90℃ under different CO_2 partial pressure a) 0.5MPa b) 1.0MPa c) 2.5MPa d) 4.0MPa

The 3D Laser Scanning Confocal Microscope was performed to further observe the pitting corrosion and to express local corrosion significantly of P110 steel. Some characteristic parameters of pitting corrosion such as pitting depth, width and density could be obtained from the 3D photographs. The characteristic parameters of pitting corrosion were listed in Table 3 and the evaluations of pitting corrosion level were according to the standard pattern [32].

Pitting coefficient represents the ratio of maximum pitting depth and average corrosion depth which was obtained from weight loss test. This coefficient was used to evaluate the sensitivity of pitting corrosion. When the pitting coefficient is higher than 1, the corrosion type of the specimens is pitting corrosion. A higher pitting coefficient means more obvious pitting corrosion.

Pitting corrosion characteristic parameters at 90℃ such as maximum pitting corrosion depth, average pitting depth and pitting coefficient were all bigger than that at 110℃, which indicated that the severity of pitting corrosion increased with the increasing of temperature. Comparing to the standard pattern, pitting depth and size were both on the first level. However, the density of corrosion hole was nearly on the top level. From the overall, the pitting corrosion of P110 steel in oilfield produced water at 90℃ and 110℃ was extremely serious.

Table 3. Pitting corrosion characteristic parameters of P110 steel in oilfield produced water

T/℃	p_{CO_2}/MPa	Max Pitting Depth/mm	Average Pitting Depth/mm	Pitting Coefficient	Size/mm^2	Density
90	0.5	0.1336	0.0955	29.31	0.0537	A5
	1.0	0.1579	0.1171	48.46	0.0792	A5
	2.5	0.0860	0.0548	11.22	0.0326	A5
	4.0	0.0699	0.0435	9.05	0.0224	A5
110	0.5	0.1522	0.1160	48.82	0.0543	A4
	1.0	0.1597	0.1428	50.12	0.0845	A5
	2.5	0.2351	0.1860	54.13	0.0586	A5
	4.0	0.2358	0.1620	63.88	0.0386	A5

Note: Pitting Coefficient=Maximum Pitting Depth / Average Corrosion Depth

3.2 Electrochemical analyses

It can be known from the weight loss tests and the surface morphology of the specimens that the most serious general corrosion happened at 60℃ and obvious local corrosion appeared at 90℃. So electrochemical tests and surface analysis were conducted at the conditions of 60℃ and 90℃ to study the corrosion mechanism of P110 in simulated oilfield produced water.

3.2.1 Results at 60℃

The potentiodynamic tests were performed to study characteristics of the anodic and cathodic reactions of electrodes with and without corrosion products. Figure 4 is the polarization curves of P110

steel at the beginning and the end of the test at 60℃. It is obviously that the corrosion potential hardly changed in the whole test process. With the increasing of CO_2 partial pressure and immersion time, the corrosion current increased. The CO_2 partial pressure had a significant effect on the cathodic process at initial time. The influences of CO_2 partial pressure retarded over time. Electrochemical corrosion kinetics parameters such as corrosion potential (E_{corr}), anodic and cathodic Tafel slopes (b_a, b_c) and corrosion current density (i_{corr}) were listed in Table 4.

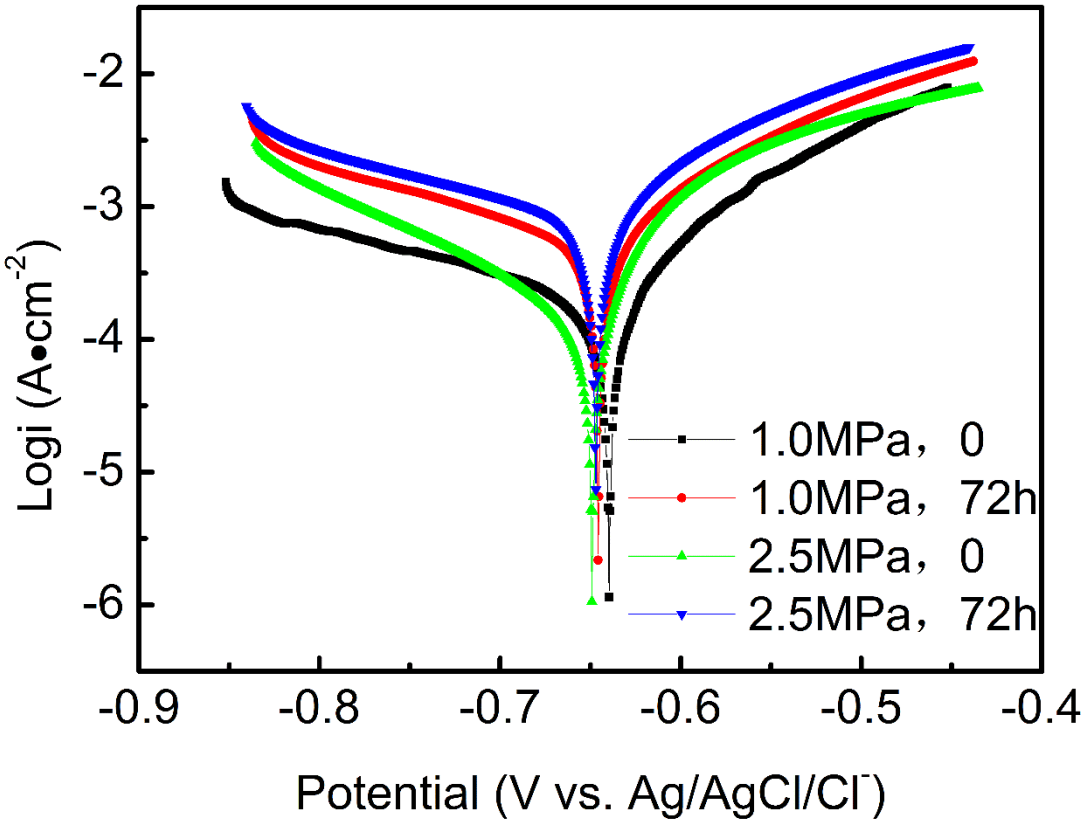

Figure 4. Polarization curves of P110 steel at 60℃ under different CO_2 partial pressure

Table 4 showed that the corrosion potential stayed on a steady level relatively. The Tafel slopes of anode and cathode both increased after immersed in the oilfield produced water for 72 hours. Relatively speaking, the anodic Tafel slopes b_a barely changed, which indicated that the anodic reaction didn't change in the test process. On the contrary, the cathodic Tafel slopes b_c changed a lot, it can be said that the corrosion products make a difference to cathodic reactions, which means that the mechanism of the cathodic reactions changes with the corrosion proceeding. The cathodic slopes b_c were much bigger than anodic slopes b_a at the same test conditions. That is to say, the corrosion process was mainly dominated by cathode reaction in this condition.

Table 4. Results of polarization curve fitting at different conditions in oilfield produced water

p_{CO_2}/ MPa	Time /h	E_{corr}/mV (vs. Ag/AgCl)	b_a/ mV·dec^{-1}	b_c/ mV·dec^{-1}	i_{corr}/ μA·cm^{-2}	R_p /Ω·cm^2
1.0	0	-640	139	199	103	88
	72	-646	155	249	495	34
2.5	0	-649	146	160	147	125
	72	-647	164	279	742	25

After 72 hours, the corrosion current density under 1.0MPa increased from 103 μA·cm^{-2} to 495 μA·cm^{-2} and it increased from 147 μA·cm^{-2} to 742 μA·cm^{-2} under 2.5 MPa. The polarization resistance R_p decreased as response. It could be concluded that P110 steel was on a very serious corrosion level at 60℃.

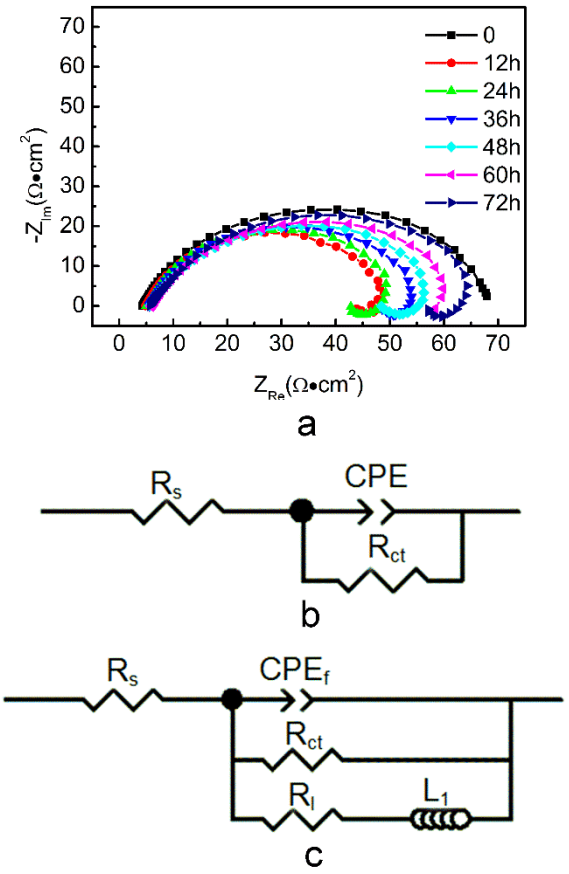

Figure 5. Nyquist diagrams of p110 steel at 60℃， p_{CO_2}=1.0 MPa and the Electrochemical equivalent circuits, R_s, Solution resistance; CPE, Constant phase element; R_{ct}, charge transfer resistance; R_l, Inductance resistance; L_1, Inductance

Figure 5a showed the results of EIS tests of P110 steel at different immersion time. At the initial immersion stage, the Nyquist curve only contained a single capacitive semicircle over the whole frequency range because of the smooth surface of specimen and the absence of corrosion product. With the corrosion proceeding, the Nyquist curve contained a capacitive semicircle in the high

frequency region and an obvious inductive arc in the low frequency region, which corresponded to two time constants. Comparing the Nyquist curve at different time, the capacitive arc had a greater radius corresponding to a relatively lower corrosion rate. The radius of the capacitive arc decreased means the corrosion rates of P110 steel increased in simulated oilfield produced water after immersing 12h. For the Nyquist curve with only one time constant, a three-element equivalent circuit (Fig. 5b) was used to fit. A five-element equivalent circuit (Fig. 5c) was used to fit the Nyquist curve with two time constants. The impedance parameters obtained by circuit fitting are listed in Table 5.

Charge-transfer resistance R_{ct} is usually used to evaluate the corrosion resistance of the electrode. The higher R_{ct} means the greater resistance of metal ionization process, which indicates the better corrosion resistance of metallic materials. At the initial stage of immersion, R_{ct} was 77 $\Omega \cdot cm^2$, which was higher than the other followed values. After the electrode immersed in the oilfield produced water for 12 hours, R_{ct} decreased to 48 $\Omega \cdot cm^2$. And then, the value of Rct increased as the experiment went on and almost the same as the initial value in the end. In the first 12 hours of the experiment, there were not corrosion products on the surface of electrode and the electrode contacted the corrosive electrolyte directly. So the corrosion rate increased sharply. With the corrosion proceeding, corrosion products accumulated on the electrode surface and form a corrosion product scale, which retard the corrosion of electrode. So the value of R_{ct} increased. However, all the values of R_{ct} were low in general, and the corrosion rates were fast, which were very identical to the results of weight loss test at 60℃. On the other hand, the value of R_{dl} increased in the whole testing process. The reason of this may be the formation and growth of corrosion product scale.

Table 5. Electrochemical impedance parameters fitted from the measured EIS data at different immersion time in oilfield produced water

Time/h	R_s/ $\Omega \cdot cm^2$	CPE/ $\mu F \cdot cm^{-2}$（n）	R_{ct}/ $\Omega \cdot cm^2$	R_1/ $\Omega \cdot cm^2$	L_1/ $H \cdot cm^{-2}$
0	4.4	98(0.8)	77	-	-
12	4.9	142(0.8)	48	215	106
24	5.1	155(0.8)	52	180	107
36	5.6	174(0.8)	54	210	159
48	5.7	196(0.7)	60	178	126
60	6.0	199(0.7)	64	186	126
72	5.7	202(0.7)	71	196	144

Surface analysis had been carried out to further understand the surface properties, morphology and their effects on electrochemical corrosion behavior. The SEM micrographs showed that some corrosion products were evenly distributed on the surface. It could be concluded from the XRD result that the corrosion product was $FeCO_3$. $FeCO_3$ distributed on the specimen sparsely, which speeded up instead of retarding the corrosion of P110 steel. Although Nesic[12] reported that $FeCO_3$ can be protective under certain conditions, the conditions are critical. $FeCO_3$ would be dangerous when the

rate of $FeCO_3$ formation is slower than the rate of corrosion. That means the protectiveness of FeCO3 is relying on its growth rate. R.A. De Motte [33] thought that the rate of corrosion and the local degree of saturation both play an important role in the initial stage of precipitation of $FeCO_3$. The predominant reactions on the corrosion process were shown below [6,12,15,34,35]:

$$CO_2(g) \rightarrow CO_2(aq) \quad (3)$$

$$CO_2 + H_2O \rightarrow H_2CO_3 \quad (4)$$

$$\mathrm{Fe} \rightarrow Fe^{2+} + 2e \quad (5)$$

$$Fe^{2+} + H_2CO_3 \rightarrow FeCO_3 + 2H^+ \quad (6)$$

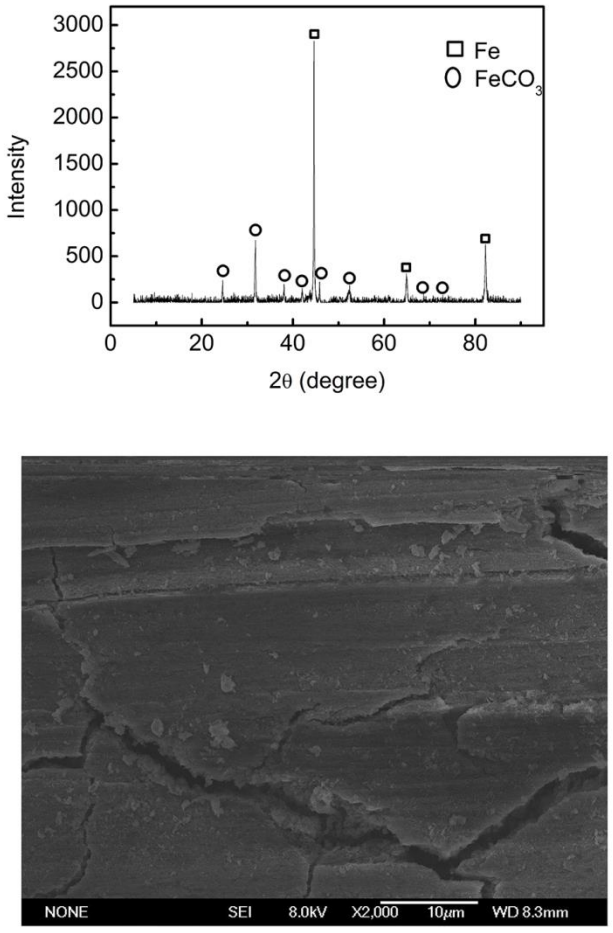

Figure 6. SEM micrograph and XRD pattern of P110 steel at 60℃ and p_{CO_2}=1.0 MPa

3.2.2 Results at 90℃

The polarization curves of P110 steel at the beginning and the end of the test at 90℃ was presented in Figure 7. Results of fitting polarization curve were listed in Table 6. Unlike at 60℃, the corrosion potential shifted in varying degrees with the increasing of CO_2 partial pressure and the extension of immersion time. The corrosion potential shifted towards the negative direction from -516 mV to -599 mV at 1.0 MPa as showed in Table 4. However, the corrosion potential at 2.5 MPa shifted towards the positive direction from -612 mV to -574 mV. The anodic Tafel slope b_a barely changed,

while the cathodic Tafel slope b_c had a relatively larger change. So the experiment conditions had a more significant effect on the cathodic process. Furthermore, the cathodic Tafel slopes b_c were bigger than the anodic Tafel slopes b_a, which indicated that the cathodic process was dominated in the electrode reaction. On the other hand, the corrosion current density all decreased after immersed for 72h at different CO_2 partial pressures. The corrosion current density under 2.5 MPa was higher than that under 1.0MPa. That is, the corrosion rate was faster in the initial time, and decreased with the corrosion proceeding. Corrosion rate would be accelerated by raising the CO_2 partial pressure.

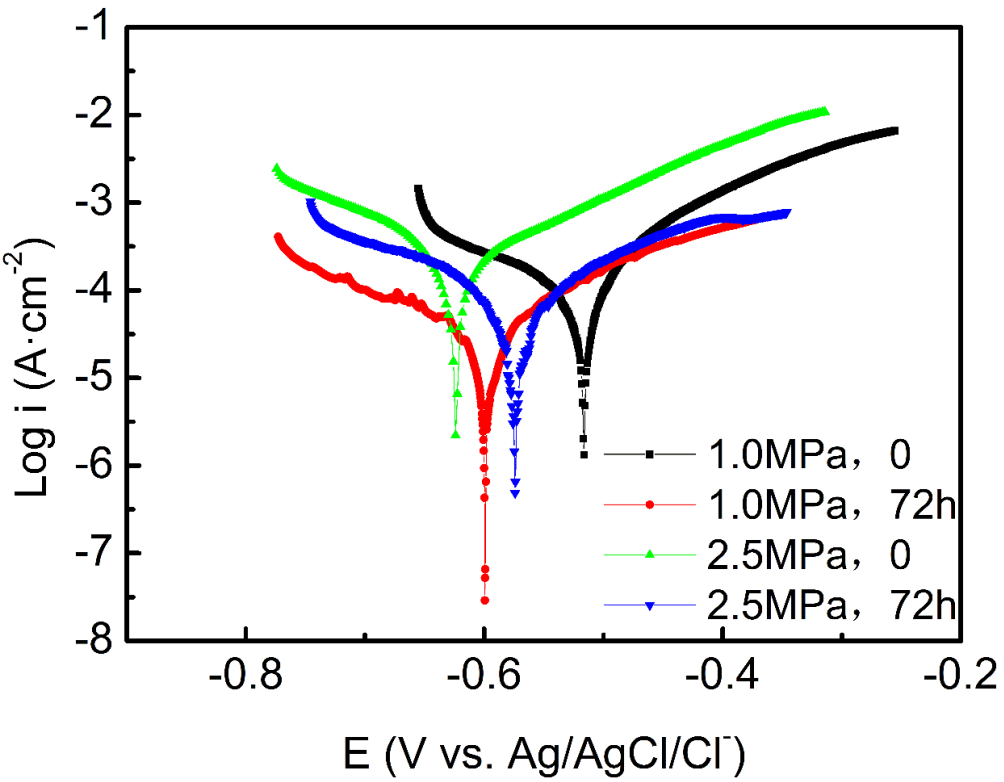

Figure 7. Polarization curves of P110 steel at 90℃ under different CO_2 partial pressure

Figure 8a shows the Nyquist curves of P110 steel electrode at the condition of 90℃ and 1.0 MPa CO_2 partial pressure for different immersion time. A five-element equivalent circuit (Fig. 8b) was used to fit and the results were listed in Table 7. At the initial stage of experiment, the impedance arc had a small radius and the charge-transfer resistance R_{ct} was 47 $\Omega \cdot cm^2$. As the experiment continued, the radius of the impedance arc increased sharply, which indicated the decreasing of corrosion rates. Besides the initial stage of the test, the charge-transfer resistances Rct at 90 were bigger 2 to 3 times than that at 60℃. These results are consistent with the data of weight loss. The reasons behind this phenomenon might be caused by corrosion products. The SEM micrograph and XRD pattern were presented in Figure 9. It could be obtained from the surface analysis that there was a dense layer of corrosion products on the surface of electrode. The main components of corrosion products was Fe_2O_3, and there was also a small amount of $Mg_3Ca(CO_3)_4$.

Table 6. Results of polarization curve fitting at different conditions in oilfield produced water at 90℃

p_{CO_2}/ MPa	Time/ h	E_{corr}/mV(vs. Ag/Cl)	b_a/mV·dec^{-1}	-b_c/mV·dec^{-1}	i_{corr}/μA·cm^{-2}	R_p/Ω·cm^2
1.0	0	-516	172	181	99	243
	72	-599	177	205	34	625
2.5	0	-612	161	190	195	113
	72	-574	162	248	114	394

Table 7. Electrochemical impedance parameters fitted from the measured EIS data at different immersion time in oilfield produced water

Time/ h	R_s/Ω·cm^2	CPE1/μF·cm^{-2} (n_1)	R_{ct}/Ω·cm^2	R_1/Ω·cm^2	CPE2/μF·cm^{-2} (n_1)
0	3.3	118(0.7)	47	-	-
12	3.8	122(0.8)	110	143	262(0.8)
24	3.7	84(0.8)	138	178	237(0.8)
36	3.9	76(0.9)	169	185	206(0.9)
48	3.8	75(0.9)	177	206	235(0.8)
60	8.7	81(0.9)	192	220	282(0.8)
72	3.9	81(0.9)	213	247	249(0.8)

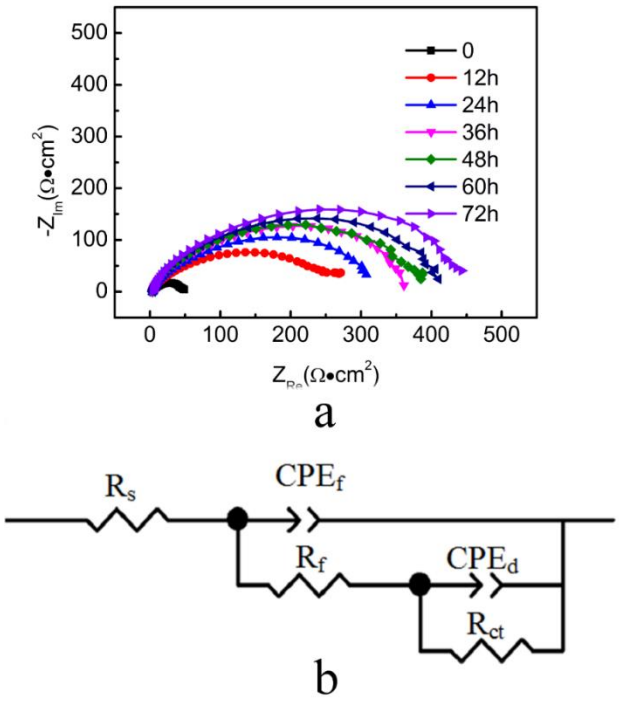

Figure 8. Nyquist diagrams of p110 steel at 90℃， p_{CO_2}=1.0 MPa and the Electrochemical equivalent circuits, Rs, solution resistance; CPE, constant phase element; R_{ct}, charge-transfer resistance; R_f, resistance of corrosion product film

At the initial stage of experiment, there was no corrosion product on the electrode, and the electrode directly contacted with the electrolyte leading to a high corrosion rate. As experiment proceeding, Fe_2O_3 gradually overlay the surface of electrode, which made the corrosion rate decrease. The resistance of corrosion product film R_1 increased gradually. The change of R_1 illustrated that the corrosion product film thickened gradually during the test process, which slowed down the corrosion rate.

Fe_2O_3 film is usually dense enough to slow down the corrosion of metallic materials. So when the product film transformed from $FeCO_3$ to Fe_2O_3, the corrosion rate decreased sharply, and this fitted well with the weight loss results and the change of the charge-transfer resistances Rct. At 90℃, a small amount of $Mg_3Ca(CO_3)_4$ was found on the corrosion product film. The existence of impurity $Mg_3Ca(CO_3)_4$ wrecked the dense structure of Fe_2O_3 film. Sun[36] believed that the inhomogeneous precipitation cased the initiation of localized corrosion. Pitting corrosion occurred in these defective areas.

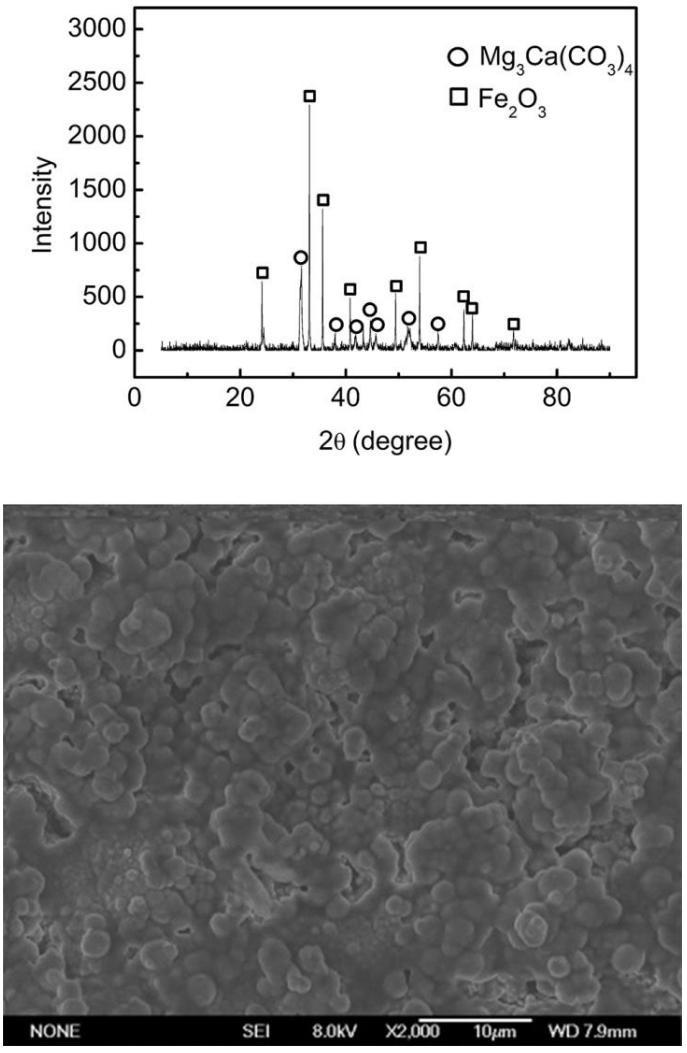

Figure 9. SEM micrograph and XRD pattern of P110 steel at 90℃ and p_{CO_2}=1.0 MPa

3.3 Discussion

The temperature and the CO_2 partial pressure both had the ability to change the corrosion style and corrosion rate of P110 steel in simulated oilfield produced water. The temperature affected the steel corrosion by controlling the formation and diversification of the corrosion products film. At 60℃ , the corrosion product film was porous and widespread $FeCO_3$ which speeded up the corrosion rates instead of retarding. As reported by Elgaddafi[20], uniform corrosion is predominant for CO_2 corrosion at low temperature (38℃) and high-pressure condition. At 90℃, the mainly corrosion product was Fe_2O_3, the product film was dense and adhering. And as a result it slowed down the corrosion rates significantly. Whereas the inhomogeneous precipitation $Mg_3Ca(CO_3)_4$ cased the initiation of localized corrosion. So the temperature could change the corrosion style from uniform corrosion to pitting corrosion by controlling the corrosion products whereas the pressure just changes the corrosion rate. At low temperature (40℃, 60℃ and 80℃), CO_2 partial pressure had a substantial impact on the corrosion rates. The influence of CO_2 partial pressure on corrosion rates became weak when the test temperature exceeded 80℃, and it could hardly affect the corrosion rates at 110℃ but it exacerbated the pitting corrosion.

4. CONCLUSIONS

1. As the temperature increased, the corrosion of P110 steel increased until it reached a peak value, and then decreased. Regardless of CO_2 partial pressure, the maximum corrosion rate was found at 60℃.
2. The existence of CO_2 enhanced the corrosion of P110 steel. At lower temperature, it affected the corrosion significantly, and this effect weakened at high temperature (90℃).
3. The temperature was the determining factor of pitting corrosion, while the CO_2 partial pressure could exacerbate the pitting corrosion.
4. At 60℃ the incomplete $FeCO_3$ film enhanced the general corrosion. At 90℃, the corrosion products were Fe_2O_3 and $Mg_3Ca(CO_3)_4$. The dense Fe_2O_3 film restrained the general corrosion, while the existence of $Mg_3Ca(CO_3)_4$ induced the pitting corrosion.

ACKNOWLEDGEMENTS
This work was supported by the National Natural Science Foundation of China (No. U1706221).

References

1. C. De Waard, U. Lotz, D. Milliams, *Corrosion*, 47 (1991) 976.
2. L. Yucheng, Z. Yinlong, Y. Jianmei, Y. Mengjing, X. Junzhong, *Eng. Failure Anal.*, 34 (2013) 35.
3. B. Tian, Y. Cheng, *Corros. Sci.*, 50 (2008) 773.
4. Y. Cai, P. Guo, D. Liu, S. Chen, J. Liu, *Sci. China: Technol. Sci.*, 53 (2010) 2342.
5. Y. Hua, R. Barker, A. Neville, *Int. J. Greenhouse Gas Control*, 31 (2014) 48.

6. Y. Zhang, M. Du, J. Zhang, J. Du, *Mater. Corros.*, 66 (2015) 366.
7. Y. Xie, L. Xu, C. Gao, W. Chang, M. Lu, *Mater. Des.*, (1980-2015) 36 (2012) 54.
8. S. Zhu, A. Fu, J. Miao, Z. Yin, G. Zhou, J. Wei, *Corros. Sci.*, 53 (2011) 3156.
9. M.H. Nazari, S. Allahkaram, M. Kermani, *Mater. Des.*, 31 (2010) 3559.
10. Y. El Mendili, A. Abdelouas, G. Karakurt, A.A. Chaou, R. Essehli, J.-F. Bardeau, J.-M. Grenèche, *Appl. Geochem.*, 52 (2015) 76.
11. D. Li, D. Han, L. Zhang, M. Lu, L. Wang, W. Ma, Effects of Temperature on CO_2 Corrosion of Tubing and Casing Steel, CORROSION 2013. NACE International, 2013.
12. S. Nešić, *Corros. Sci.*, 49 (2007) 4308.
13. G. Zhang, Y. Zeng, X. Guo, F. Jiang, D. Shi, Z. Chen, *Corros. Sci.*, 65 (2012) 37.
14. W.-f. LI, Y.-J. Zhou, X. Yan, *J. Iron Steel Res. Int.*, 19 (2012) 59.
15. G. Zhang, Y. Cheng, *Corros. Sci.*, 51 (2009) 1589.
16. Y. Zhang, X. Pang, S. Qu, X. Li, K. Gao, *Corros. Sci.*, 59 (2012) 186.
17. Y.-S. Choi, F. Farelas, S. Nešić, A.A.O. Magalhães, C. de Azevedo Andrade, *Corrosion*, 70 (2013) 38.
18. Y. Xiang, Z. Wang, Z. Li, W.D. Ni, *Corros. Eng., Sci. Technol.*, 48 (2013) 121.
19. Y.-S. Choi, S. Nešić, *Int. J. Greenhouse Gas Control*, 5 (2011) 788.
20. R. Elgaddafi, R. Ahmed, S. Hassani, S. Shah, S.O. Osisanya, *J. Pet. Sci. Eng.*, 146 (2016) 777.
21. H. Karimi Abadeh, M. Javidi, *J. Nat. Gas Sci. Eng.*, 67 (2019) 93.
22. A.S. Yaro, K.R. Abdul-Khalik, A.A. Khadom, *J. Loss Prev. Process Ind.*, 38 (2015) 24.
23. D. Ekawati, T. Berntsen, M. Seiersten, T. Hemmingsen, *Corrosion*, 73 (2017) 1157.
24. Y. Hua, A. Shamsa, R. Barker, A. Neville, *Appl. Surf. Sci.*, 455 (2018) 667.
25. H. Mansoori, D. Young, B. Brown, M. Singer, *J. Nat. Gas Sci. Eng.*, 59 (2018) 287.
26. K. Gao, F. Yu, X. Pang, G. Zhang, L. Qiao, W. Chu, M. Lu, *Corros. Sci.*, 50 (2008) 2796.
27. F.F. Eliyan, A. Alfantazi, *Corros. Sci.*, 85 (2014) 380.
28. M. Gao, X. Pang, K. Gao, *Corros. Sci.*, 53 (2011) 557.
29. M. Xu, W. Li, Y. Zhou, X. Yang, Z. Wang, Z. Li, *Int. J. Greenhouse Gas Control*, 51 (2016) 357.
30. K. Deng, Y. Lin, H. Ning, W. Liu, A. Singh, G. Zhang, *Appl. Geochem.*, 99 (2018) 22.
31. L.M. Tavares, E.M.d. Costa, J.J.d.O. Andrade, R. Hubler, B. Huet, *Appl. Surf. Sci.*, 359 (2015) 143.
32. A. Standard, (2005).
33. R.A. De Motte, R. Barker, D. Burkle, S.M. Vargas, A. Neville, *Mater. Chem. Phys.*, 216 (2018) 102.
34. J. Li, H. Ma, S. Zhu, C. Qu, Z. Yin, *Corros. Sci.*, 86 (2014) 101.
35. N. Lin, F. Xie, J. Zhou, X. Wu, W. Tian, *J. Wuhan Univ. Technol., Mater. Sci. Ed.*, 26 (2011) 190.
36. C. Sun, J. Sun, Y. Wang, P. Sui, X. Lin, H. Liu, X. Cheng, M. Zhou, *Int. J. Greenhouse Gas Control*, 65 (2017) 117.